
<https://doi.org/10.15407/ujpe70.4.263>

N.I. PAVLYSHCHE,¹ A.V. KOROTUN,^{1,2} V.P. KURBATSKY,¹ V.I. REVA¹

¹ National University “Zaporizhzhia Polytechnic”

(64, Zhukovs'kogo Str., Zaporizhzhya 69063, Ukraine; e-mail: andko@zp.edu.ua)

² G.V. Kurdyumov Institute for Metal Physics, Nat. Acad. of Sci. of Ukraine

(36, Akademika Vernads'kogo Blvd., Kyiv 03142, Ukraine)

PLASMON PHENOMENA IN METAL-DIELECTRIC NANODISCS. AN EQUIVALENT-SPHEROID APPROACH

In the framework of the equivalent-spheroid approach, the expressions for the diagonal components of the polarizability tensor and the extinction efficiency, as well as the size dependences of the longitudinal and transverse surface plasmon resonance frequencies for metal-dielectric nanodisks, have been obtained. The results of calculations of the indicated characteristics are presented for disks of various sizes. The influence of the core and shell materials and the disk sizes on the position and magnitude of the extinction efficiency maximum has been analyzed. The reason for why only one maximum in the extinction spectra of metal-dielectric nanodisks is detected has been determined.

Key words: metal-dielectric nanodisk, polarizability tensor, extinction efficiency, relaxation rate, surface plasmon resonance.

1. Introduction

Metal nanoparticles exhibit extremely interesting optical properties due to the excitation of localized surface plasmon resonance (SPR), which is defined as a collective motion of conduction electrons induced by an electromagnetic field [1]. In turn, the localized SPRs of metal nanoparticles can induce unusual optical absorption and scattering and enhance electric fields near the nanoparticle surface. Furthermore, the localized SPRs of metal nanoparticles have been found sensitive to their geometry and the surrounding environment [2–7]. To date, various metallic nanostructures such as rods or wires [8, 9], shells [10, 11], cups [12], tubes [13], rings [14], are in study

[15], and three-layer nanodisks [16] have been proposed for various applications.

Substantial progress has been achieved in the synthesis of compounds involving silica composites with plasmonic particles [17–21] targeted at specific applications including batteries or photovoltaic cells [22–25], plasmonic waveguides [26], biological sensors [27, 28], and so forth. In this regard, considerable efforts have been directed to reveal the optical properties of the systems consisting of crystalline structures or composite materials, such as “metal core–dielectric shell” systems [29–32].

It is known that the spatial structures of plasmon modes in disk-shaped nanoparticles are much more complicated. For instance, owing to an increase in the volume damping effect [33], the spectral widths of individual modes in nanodisks become wider as compared to the nanorod case. As a result, the overlapping of plasmon resonances [34, 35] can take place.

However, experimentally, surface plasmons in metal-dielectric disks have been researched insuffi-

Citation: Pavlyshche N.I., Korotun A.V., Kurbatsky V.P., Reva V.I. Plasmon phenomena in metal-dielectric nanodisks. An equivalent-spheroid approach. *Ukr. J. Phys.* **70**, No. 4, 263 (2025). <https://doi.org/10.15407/ujpe70.4.263>.

© Publisher PH “Akademperiodyka” of the NAS of Ukraine, 2025. This is an open access article under the CC BY-NC-ND license (<https://creativecommons.org/licenses/by-nc-nd/4.0/>)

ISSN 2071-0194. *Ukr. J. Phys.* 2025. Vol. 70, No. 4

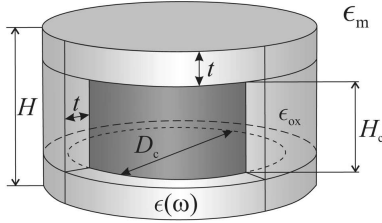


Fig. 1. Geometry of the problem. See explanations in the text

ciently, and the corresponding theoretical studies have not been carried out at all. Therefore, the research of the optical response of metal disks covered with a dielectric layer is challenging.

2. Basic Relationships

Let us consider a nano-sized disk with diameter D and height of H , which consists of a metal core covered with a dielectric layer of thickness t . Let us assume that the nanodisk is in a medium with dielectric permeability ϵ_m , and the dielectric permeability of the dielectric disk shell equals ϵ_s (Fig. 1).

Since the disk sizes are much smaller than the length of the incident light wave, the optical (plasmon) properties can be studied in the quasi-static approximation. However, analytic solutions to the boundary value problems for the Laplace equation exist only for a limited number of cases (the spherical or spheroidal geometry). In the other cases, numerical methods are applied, or the nanoparticle is represented by a similar-in-shape spheroid. In particular, in works [36, 37] this approach was used to study the optical (plasmon) properties of metal nanodisks. The particle under study was assumed to correspond to a spheroid with the aspect ratio equal to the ratio between the longitudinal and transverse sizes of this particle. However, in work [38] it was shown that, closer to the real situation, is the equivalent-spheroid method, in which the nanoparticle is replaced by a spheroid with the effective aspect ratio found from the equality of the ratio between the moments of inertia with respect to the corresponding axes of the particle and the analogous ratio for the spheroid. In particular, the calculations of the longitudinal surface plasmon resonance frequencies carried out for a cylinder using this method showed a better agreement with the experiment [38, 39] than the corresponding calculations in the framework of the similar-

in-shape spheroid approach. Therefore, when studying the plasmonic properties of metal-dielectric nanodisks, we will use the approach of an equivalent oblate spheroid.

According to the aforesaid, the optical properties of a two-layer nanodisk will be described by the relationship for the polarizability of an equivalent metal-dielectric spheroid

$$\alpha_{\text{@}}^{\perp(\parallel)} = V \frac{\epsilon_{\text{@}}^{\perp(\parallel)}(\omega) - \epsilon_m}{\epsilon_m + \mathcal{L}_{\perp(\parallel)}^{(2)}(\epsilon_{\text{@}}^{\perp(\parallel)}(\omega) - \epsilon_m)}. \quad (1)$$

Here, the diagonal components of the dielectric tensor of the two-layer nanodisk are determined by the formula

$$\epsilon_{\text{@}}^{\perp(\parallel)}(\omega) = \epsilon_s \left[1 + \beta_c \frac{\epsilon^{\perp(\parallel)}(\omega) - \epsilon_s}{\epsilon_s + (\epsilon^{\perp(\parallel)}(\omega) - \epsilon_s)(\mathcal{L}_{\perp(\parallel)}^{(1)} - \beta_c \mathcal{L}_{\perp(\parallel)}^{(2)})} \right], \quad (2)$$

where

$$\beta_c = \frac{(D - 2t)^2 (H - 2t)}{D^2 H} \quad (3)$$

is the volume fraction occupied by the metal, the diagonal components of the dielectric tensor of the metal core equal

$$\epsilon^{\perp(\parallel)}(\omega) = \epsilon^\infty - \frac{\omega_p^2}{\omega(\omega + i\gamma_{\text{eff}}^{\perp(\parallel)})}, \quad (4)$$

ϵ^∞ is the contribution of the ionic core to the dielectric function of the metal, $\omega_p = \sqrt{e^2 n_e / \epsilon_0 m^*}$ is the bulk plasmon frequency, e is the elementary charge, $n_e = 3 / (4\pi r_s^3)$ is the electron concentration, r_s is the average distance between the electrons, ϵ_0 is the electric constant of vacuum, and m^* is the effective electron mass.

The effective relaxation rate has three components,

$$\gamma_{\text{eff}}^{\perp(\parallel)} = \gamma_{\text{bulk}} + \gamma_s^{\perp(\parallel)} + \gamma_{\text{rad}}^{\perp(\parallel)}, \quad (5)$$

where $\gamma_{\text{bulk}} = \tau_{\text{bulk}}^{-1}$ is the bulk relaxation rate, which is a constant for a particular metal,

$$\gamma_s^{\perp(\parallel)} = \mathcal{A}_{\perp(\parallel)} \frac{v_F}{l_{\perp(\parallel)}} \quad (6)$$

is the surface relaxation rate, and

$$\gamma_{\text{rad}}^{\perp(\parallel)} = \mathcal{B}_{\perp(\parallel)} \frac{v_F}{l_{\perp(\parallel)}} \quad (7)$$

is the radiative decay rate. In formulas (6) and (7), v_F is the Fermi velocity of electrons, $l_{\parallel} = H - 2t$ and $l_{\perp} = D - 2t$ are the longitudinal and transverse sizes of the metal core. The size-dependent multipliers are as follows:

$$\mathcal{A}_{\perp(\parallel)} = \frac{9}{16} \frac{\mathcal{L}_{\perp(\parallel)}^{(1)}}{\epsilon_m + \mathcal{L}_{\perp(\parallel)}^{(1)} (1 - \epsilon_m)} \left(\frac{\omega_p}{\omega}\right)^2 \mathcal{F}_{\perp(\parallel)}(\varrho_{\text{eff}}^{(1)}), \quad (8)$$

$$\mathcal{B}_{\perp(\parallel)} = \frac{9V}{128\pi} \frac{\mathcal{L}_{\perp(\parallel)}^{(1)}}{\sqrt{\epsilon_m \left[\epsilon^{\infty} + \left(\frac{1}{\mathcal{L}_{\perp(\parallel)}^{(1)}} - 1\right) \epsilon_m \right]}} \times \left(\frac{\omega_p}{c}\right)^3 \left(\frac{\omega_p}{\omega}\right)^2 \mathcal{F}_{\perp(\parallel)}(\varrho_{\text{eff}}^{(1)}), \quad (9)$$

from where, the depolarization factors $\mathcal{L}_{\perp(\parallel)}^{(1,2)}$ for oblate spheroids are determined by the formulas

$$\mathcal{L}_{\parallel}^{(1,2)} = \frac{\left[\varrho_{\text{eff}}^{(1,2)}\right]^2}{\left(\left[\varrho_{\text{eff}}^{(1,2)}\right]^2 - 1\right)^{\frac{3}{2}}} \times \left(\sqrt{\left[\varrho_{\text{eff}}^{(1,2)}\right]^2 - 1} + \arctan \frac{1}{\sqrt{\left[\varrho_{\text{eff}}^{(1,2)}\right]^2 - 1}} - \frac{\pi}{2} \right), \quad (10)$$

$$\mathcal{L}_{\perp}^{(1,2)} = \frac{1}{2} \left(1 - \mathcal{L}_{\parallel}^{(1,2)}\right), \quad (11)$$

and the functions $\mathcal{F}_{\perp(\parallel)}(\varrho_{\text{eff}}^{(1)})$ looks like [40]

$$\mathcal{F}_{\perp}(\varrho_{\text{eff}}^{(1)}) = \frac{1}{2} \left(\varrho_{\text{eff}}^{(1)2} - 1\right)^{-\frac{3}{2}} \times \left\{ \varrho_{\text{eff}}^{(1)} \left(2\varrho_{\text{eff}}^{(1)2} - 3\right) \sqrt{\varrho_{\text{eff}}^{(1)2} - 1} + \left(4\varrho_{\text{eff}}^{(1)2} - 3\right) \ln \left(\varrho_{\text{eff}}^{(1)} + \sqrt{\varrho_{\text{eff}}^{(1)2} - 1}\right) \right\}, \quad (12)$$

$$\mathcal{F}_{\parallel}(\varrho_{\text{eff}}^{(1)}) = \left(\varrho_{\text{eff}}^{(1)2} - 1\right)^{-\frac{3}{2}} \times \left\{ \varrho_{\text{eff}}^{(1)} \left(2\varrho_{\text{eff}}^{(1)2} - 1\right) \sqrt{\varrho_{\text{eff}}^{(1)2} - 1} - \ln \left(\varrho_{\text{eff}}^{(1)} + \sqrt{\varrho_{\text{eff}}^{(1)2} - 1}\right) \right\}. \quad (13)$$

The effective aspect ratios equal [40]

$$\varrho_{\text{eff}}^{(1,2)} = \frac{\sqrt{3}}{2} \varrho^{(1,2)}, \quad (14)$$

where the aspect ratios for the entire disk and the metal core are, respectively,

$$\varrho^{(2)} = \frac{D}{H}, \quad \varrho^{(1)} = \frac{D - 2t}{H - 2t}. \quad (15)$$

Finally, the frequencies of transverse (longitudinal) surface plasmon resonances are found from the condition that the real part of the denominator in expression (1) equals zero. In the dissipative approximation ($\gamma_{\text{eff}}^{\perp(\parallel)} \rightarrow 0$), we obtain

$$\omega_{sp}^{\perp(\parallel)} = \frac{\omega_p}{\sqrt{\epsilon^{\infty} - \frac{\epsilon_m - \frac{\epsilon_s}{\beta_c} \left(1 + \frac{\epsilon_m}{\epsilon_s} \frac{1 - \mathcal{L}_{\perp(\parallel)}^{(2)}}{\mathcal{L}_{\perp(\parallel)}^{(2)}}\right) (1 - \mathcal{L}_{\perp(\parallel)}^{(1)} + \beta_c \mathcal{L}_{\perp(\parallel)}^{(2)})}{1 + \frac{1}{\beta_c} \left(1 + \frac{\epsilon_m}{\epsilon_s} \frac{1 - \mathcal{L}_{\perp(\parallel)}^{(2)}}{\mathcal{L}_{\perp(\parallel)}^{(2)}}\right) (\mathcal{L}_{\perp(\parallel)}^{(1)} - \beta_c \mathcal{L}_{\perp(\parallel)}^{(2)})}}}. \quad (16)$$

Note that according to formula (16), the frequencies of the longitudinal and transverse SPRs depend on three dimensional parameters: two effective aspect ratios, $\varrho_{\text{eff}}^{(1)}$ and $\varrho_{\text{eff}}^{(2)}$, and the bulk metal content in the metal-dielectric disk, β_c . This fact significantly complicates the analysis of the size dependences of the SPR frequencies $\omega_{sp}^{\perp(\parallel)}$. However, the quantities β_c and $\varrho_{\text{eff}}^{(2)}$ can be expressed in terms of $\varrho_{\text{eff}}^{(1)}$ and $q = 2t/(H - 2t)$, thus reducing the number of size parameters affecting the SPR frequencies to two. From formulas (14) and (3), we obtain

$$\varrho_{\text{eff}}^{(2)} = \frac{\sqrt{3}}{2} \frac{\frac{2}{\sqrt{3}} \varrho_{\text{eff}}^{(1)} + q}{1 + q}. \quad (17)$$

$$\beta_c = \frac{\frac{4}{3} \left[\varrho_{\text{eff}}^{(1)}\right]^2 + q}{(1 + q) \left(\frac{2}{\sqrt{3}} \varrho_{\text{eff}}^{(1)} + q\right)^2}. \quad (18)$$

The absorption, scattering, and extinction cross-sections are given by the expressions

$$C_{\text{a}}^{\text{abs}} = \frac{\omega}{c} \sqrt{\epsilon_m} \left(\frac{2}{3} \text{Im} \alpha_{\text{a}}^{\perp} + \frac{1}{3} \text{Im} \alpha_{\text{a}}^{\parallel}\right), \quad (19)$$

$$C_{\text{a}}^{\text{sca}} = \frac{\omega^4}{6\pi c^4} \epsilon_m^2 \left(\frac{2}{3} |\alpha_{\text{a}}^{\perp}|^2 + \frac{1}{3} |\alpha_{\text{a}}^{\parallel}|^2\right), \quad (20)$$

$$C_{\text{a}}^{\text{ext}} = C_{\text{a}}^{\text{abs}} + C_{\text{a}}^{\text{sca}}. \quad (21)$$

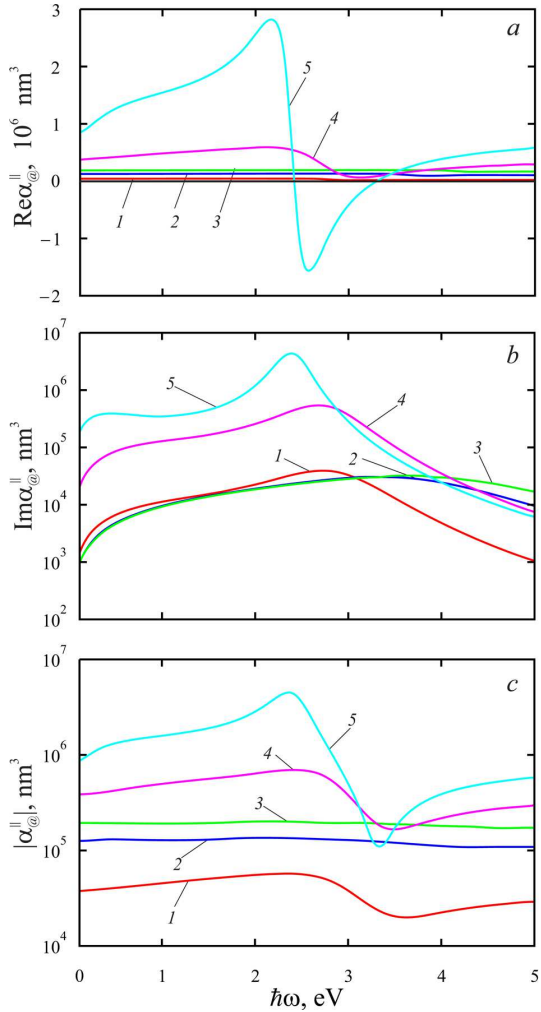


Fig. 2. Frequency dependences of the real (a) and imaginary (b) parts and the modulus (c) of the longitudinal component of the polarization tensor of Au@SiO₂ nanodisks with various sizes and a fixed dielectric shell thickness $t = 3$ nm: $D = 40$ nm, $H = 10$ nm (1); $D = 80$ nm, $H = 10$ nm (2); $D = 100$ nm, $H = 10$ nm (3); $D = 80$ nm, $H = 20$ nm (4); $D = 80$ nm, $H = 30$ nm (5)

The relationships for the optical efficiencies of absorption, scattering, and extinction look like

$$Q_{\text{@}}^{\text{abs}} = \frac{C_{\text{@}}^{\text{abs}}}{S}, \quad Q_{\text{@}}^{\text{sca}} = \frac{C_{\text{@}}^{\text{sca}}}{S}, \quad Q_{\text{@}}^{\text{ext}} = \frac{C_{\text{@}}^{\text{ext}}}{S}, \quad (22)$$

where

$$S = \pi R_{\text{eq}}^2 \quad (23)$$

is the equivalent cross-section area of the disk-like nanoparticle. The equivalent radius R_{eq} is found from

the equality of the sphere and disk volumes and is equal to [36]

$$R_{\text{eq}} = \frac{1}{2} \sqrt[3]{\frac{3}{2} D^2 H}. \quad (24)$$

While obtaining numerical results, relationships (1), (16), and (22) were used with regard for expressions (2), (4)–(14), (17)–(21), and (23), (24).

3. Calculation Results and Their Discussion

The frequency dependences of the extinction efficiency and the diagonal components of the polarization tensor, as well as the size dependences of the surface plasmon resonance frequencies, were calculated for metal-dielectric disks with various sizes. The material parameters for metals (cores) and insulators (shells) required for the calculations are quoted in Tables 1 and 2, respectively.

In Fig. 2, the frequency dependences of the real and imaginary parts and the modulus of the longitudinal component of the polarization tensor for Au@SiO₂ disks with various diameters D and heights H and a constant dielectric shell thickness t are shown. The calculation results testify that the functions $\text{Re } \alpha_{\text{@}}^{\parallel}(\omega)$ change their sign, whereas $\text{Im } \alpha_{\text{@}}^{\parallel}(\omega) > 0$ within the whole examined frequency interval. Note that, as the disk diameter D increases (at $H = \text{const}$), the maximum of $\text{Im } \alpha_{\text{@}}^{\parallel}$ shifts toward the high-frequency region (the curve sequence

Table 1. Parameters of metal cores (see, e.g., works [36, 39] and references therein)

Parameters	Metals			
	Cu	Au	Ag	Pt
r_s/a_0	2.11	3.01	3.02	3.27
m^*/m_e	1.49	0.99	0.96	0.54
ϵ^∞	12.03	9.84	3.7	4.42
$\gamma_{\text{bulk}}, 10^{14} \text{ s}^{-1}$	0.37	0.35	0.25	1.05

Table 2. Dielectric permittivities ϵ_s of dielectric shells

Parameter	Material			
	SiO ₂	ZnO	Ta ₂ O ₅	Nb ₂ O ₅
ϵ_s	2.10	4.00	4.67	6.15

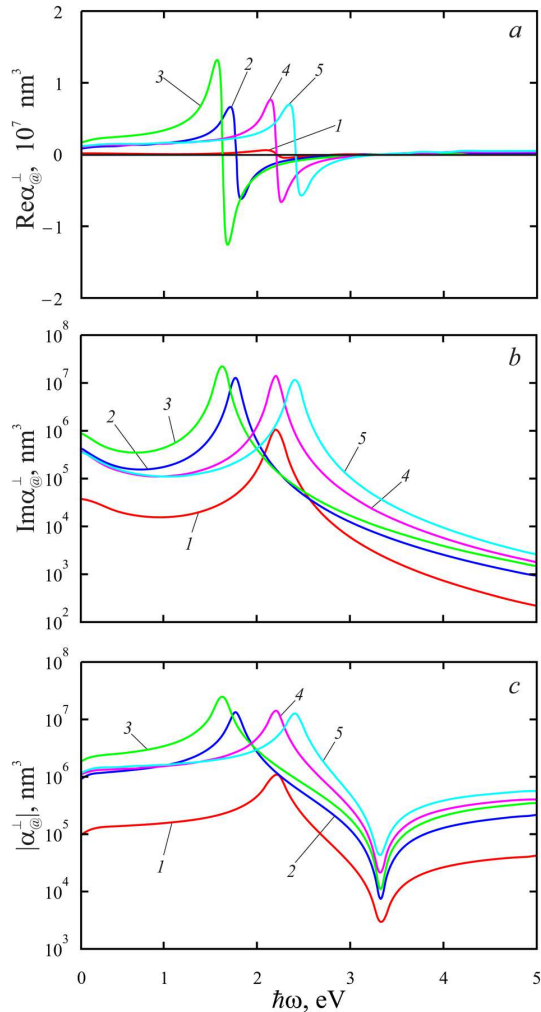


Fig. 3. The same as in Fig. 2 but for the transverse component of the polarization tensor of Au@SiO₂ nanodisks

1 → 2 → 3), and the corresponding maximum values simultaneously decrease. At the same time, as the disk height H increases (at $D = \text{const}$), a “red” shift of the maxima takes place with a simultaneous increase in their values (the curve sequence 2 → 4 → 5).

Analogous dependences for the transverse component of the polarization tensor of Au@SiO₂ disks are shown in Fig. 3. An essentially different character of the evolution of $\text{Im } \alpha_{\perp}^{\parallel}$ with the change in the nanodisk diameter and height in comparison with that of $\text{Im } \alpha_{\parallel}^{\parallel}$ should be noted. In particular, as the disk diameter D increases at $H = \text{const}$, the maximum of $\text{Im } \alpha_{\perp}^{\parallel}$ undergoes a “red” shift (the curve sequence 1 → 2 → 3) rather than a “blue” one, as in the case

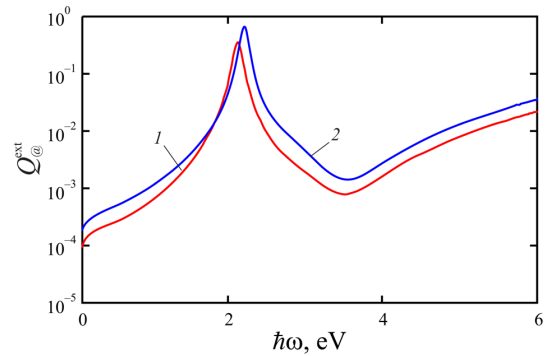


Fig. 4. Frequency dependences of the extinction efficiency for Au@SiO₂ nanospheroids (1) and nanodisks (2) with $D = 80$ nm, $H = 20$ nm, and $t = 5$ nm

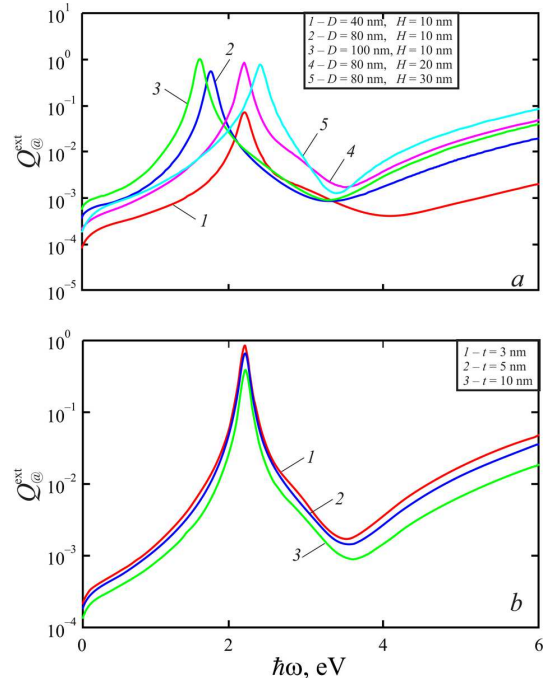


Fig. 5. Frequency dependences of the extinction efficiency of Au@SiO₂ nanodisks: with the changing sizes and the fixed dielectric shell thickness $t = 3$ nm (a); with the changing shell thickness and the fixed sizes ($D = 80$ nm, $H = 20$ nm) (b)

of $\text{Im } \alpha_{\parallel}^{\parallel}$. On the other hand, as the disk height H increases at $D = \text{const}$, the maximum of the imaginary part shifts towards the high-frequency region, but its amplitude does not change (the curve sequence 2 → 4 → 5).

The frequency dependences of the extinction efficiency for a disk and an oblate spheroid, (when the spheroid semiaxes equal the radius, and the half-

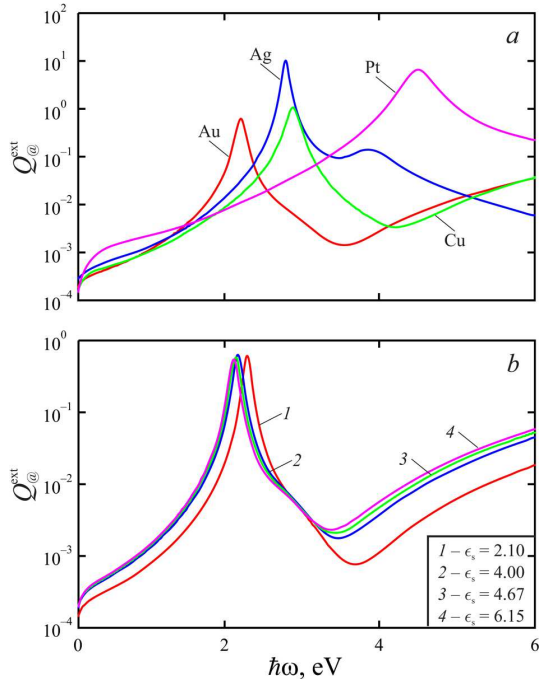


Fig. 6. Frequency dependences of the extinction efficiency for Me@SiO₂ (a) and Au@D (b) nanodisks. Nanodisk sizes are $D = 80$ nm, $H = 20$ nm, and $t = 5$ nm

Table 3. Calculated SPR frequencies at $\varrho^{(1)} = 2$

SPR frequencies	$\epsilon_s = 2,10$		$\epsilon_s = 6,15$	
	Au@SiO ₂	Cu@SiO ₂	Au@Nb ₂ O ₅	Cu@Nb ₂ O ₅
ω_{sp}^\perp , eV	2.685	3.415	2.540	3.259
ω_{sp}^\parallel , eV	2.528	3.246	2.448	3.158

height of the disk) are compared in Fig. 4. The closeness of the $Q_{\textcircled{a}}^{\text{ext}}(\omega)$ curves for the disk and the oblate spheroid testifies in favor of the equivalent-oblate-spheroid approach while studying the optical properties of nanodisks.

The evolution of the extinction spectra with the changes of the nanodisk diameter and height can be observed in Fig. 5, a. We can see that the shifts of the $Q_{\textcircled{a}}^{\text{ext}}$ maximum and the changes of its magnitude are the same as for the maximum of $\text{Im } \alpha_{\textcircled{a}}^\perp$. It should be noted that the expression for $Q_{\textcircled{a}}^{\text{ext}}(\omega)$ is characterized by the presence of two maxima for the extinction efficiency, but Figs. 4 and 5 demonstrate only one. This fact can be explained in either of two ways.

(i) As was noted in works [37, 42], the longitudinal and transverse SPRs in non-spherical nanostructures are excited at close frequencies; therefore, they do not reveal themselves in the experimental and theoretical spectra. Indeed, for the Au@SiO₂, Cu@SiO₂, Au@Nb₂O₅, and Cu@Nb₂O₅ disks at $\varrho^{(1)} = 2$, as well as for monometallic disks [37],

$$\Delta\omega_{sp} = \left| \omega_{sp}^\perp - \omega_{sp}^\parallel \right| \simeq \gamma_{\text{eff}}^\perp, \gamma_{\text{eff}}^\parallel; \quad (25)$$

therefore, the two maxima merge into one (see Table 3).

(ii) For disks made of other materials and characterized by other $\varrho^{(1)}$ -values, we have $\max \{ \text{Im } \alpha_{\textcircled{a}}^\parallel \} \ll \ll \max \{ \text{Im } \alpha_{\textcircled{a}}^\perp \}$. Therefore, the second maximum does not appear in the extinction spectra.

At the same time, an increase in the dielectric shell thickness gives rise to only a slight decrease in the extinction efficiency value within the whole examined frequency interval (Fig. 5, b).

The frequency dependences of the extinction efficiency for disks with various metal cores and various dielectric shells are shown in Fig. 6. As one can see, the maximum of $Q_{\textcircled{a}}^{\text{ext}}$ undergoes a “blue” shift along the metal series Au → Ag → Cu → Pt, which is associated with a growth of the plasma frequency (and, accordingly, the SPR frequency) along this metal series. In turn, the covering of the disk with a dielectric shell possessing a higher dielectric constant (the series SiO₂ → ZnO → Ta₂O₅ → Nb₂O₅) induces a small “red” shift of the extinction efficiency maximum.

4. Conclusions

In the framework of the equivalent-spheroid approach, relationships for the extinction efficiency and the diagonal components of the polarizability tensor for metal-dielectric disks, as well as for the frequencies of the longitudinal and transverse surface plasmon resonances, have been obtained. It is shown that, with an increase in the disk diameter or a decrease in the disk height, the amplitudes of the maxima of the imaginary parts of both the transverse and longitudinal components of the polarization tensor increase. However, in the former case, in contrast to the latter one, a “red” shift of the maximum takes place.

The closeness of the numerical values of the extinction efficiency at the same frequency for nanodisks

and oblate spheroids with the corresponding lengths of semi-axes has been demonstrated, which confirms the feasibility of using the equivalent-spheroid approach to study the optical properties of metal-dielectric disks.

It has been found that the absence of the second maximum in the extinction spectra can be explained by two reasons: (i) the merging of the maxima due to the proximity of the longitudinal and transverse SPR frequencies and (ii) the suppression of the second maximum due to the smallness of the imaginary part of the longitudinal polarization component in comparison with that of the transverse component at this resonance frequency.

It has been proved that, by changing the core metal, we can substantially affect both the position and the amplitude of the extinction efficiency maximum, which is explained by the difference in the optical characteristics of different metals.

- U. Kreibig, M. Vollmer *Optical Properties of Metal Clusters* (Springer, 1995).
- K.L. Kelly, E. Coronado, L.L. Zhao, G.C. Schatz. The Optical Properties of Metal Nanoparticles: The influence of size, shape, and dielectric environment. *J. Phys. Chem. B* **107**, 668 (2003).
- N.K. Grady, N.J. Halas, P. Nordlander. Influence of dielectric function properties on the optical response of plasmon resonant metallic nanoparticles. *Chem. Phys. Lett.* **399**, 167 (2004).
- N.I. Grigorukh. Plasmon resonant light scattering on spheroidal metallic nanoparticle embedded in a dielectric matrix. *Europhys. Lett.* **97**, 45001 (2012).
- P.M. Tomchuk. Dependence of the cross-section of light scattering by metal nanoparticles on their shape. *Ukr. Fiz. Zh.* **57**, 553 (2012) (in Ukrainian).
- M.L. Dmytruk, S.Z. Malynych. Surface plasmon resonances and their manifestation in the optical properties of nanostructures of noble metals. *Ukr. Fiz. Zh. Oglyady* **9**, 3 (2014) (in Ukrainian).
- A.O. Koval, A.V. Korotun, Yu.A. Kunitsky, V.A. Tatarenko, I.M. Titov. *Electrodynamics of Plasmon Effects in Nanomaterials*. (Naukova dumka 2021) (in Ukrainian).
- S.R. Nicewarner-Pena, R. Griffith-Freeman, B.D. Reiss, L. He, D.J. Pena, I.D. Walton, R. Cromer, C.D. Keating, M.J. Natan. Submicrometer metallic barcodes. *Science* **294**, 137 (2001).
- J.J. Mock, S.J. Oldenburg, D.R. Smith, D.A. Schultz, S. Schultz. Composite plasmon resonant nanowires. *Nano Lett.* **2**, 465 (2002).
- D.J. Wu, X.J. Liu, L.L. Liu, W.P. Qian. Third-order nonlinear optical properties of gold nanoshells in aqueous solution. *Appl. Phys. A* **92**, 279 (2008).
- G.V.P. Kumar, S. Shruthi, B. Vibha, B.A.A. Reddy, T.K. Kundu, C. Narayana. Hot spots in Ag core – Au shell nanoparticles potent for surface-enhanced Raman scattering studies of biomolecules. *J. Phys. Chem. C* **111**, 4388 (2007).
- C. Charnay, A. Lee, S.Q. Man, C.E. Moran, C. Radloff, R.K. Bradley, N.J. Halas. Reduced symmetry metallo-dielectric nanoparticles: chemical synthesis and plasmonic properties. *J. Phys. Chem. B* **107**, 7327 (2003).
- A.V. Korotun, Ya.V. Karandas. Surface plasmons in a nanotube with a finite-thickness wall. *Phys. Metals. Metallogr.* **123**, 7 (2022).
- J. Aizpurua, P. Hanarp, D.S. Sutherland, M. Kall, G.W. Bryant, F.J. Garcia de Abajo. Optical properties of gold nanorings. *Phys. Rev. Lett.* **90**, 057401 (2003).
- A.V. Korotun. Plasmonic phenomena in biconical and bipyramidal metal nanoparticles. *Ukr. Fiz. Zh.* **68**, 697 (2023) (in Ukrainian).
- K.H. Su, Q.H. Wei, X. Zhang. Tunable and augmented plasmon resonances of Au/SiO₂/Au nanodisks. *Appl. Phys. Lett.* **88**, 063118 (2006).
- O. Niitsoo, A. Couzis. Facile synthesis of silver core – silica shell composite nanoparticles. *J. Colloid Interf. Sci.* **354**, 887 (2011).
- S. Tang, Y. Tang, S. Zhu, H. Lu, X. Meng. Synthesis and characterization of silica-silver core-shell composite particles with uniform thin silver layers. *J. Solid State Chem.* **180**, 2871 (2007).
- S. Amoruso, R. Bruzzese, N. Spinelli, R. Velotta, M. Vitiello, X.Q. Wang, G. Ausanio, V. Iannotti, L. Lanotte. Generation of silicon nanoparticles via femtosecond laser ablation in vacuum. *Appl. Phys. Lett.* **84**, 4502 (2004).
- S.L. Zhu, L. Tang, Z.D. Cui, Q. Wei, X.J. Yang. Replication of copper-coated β -SiC nanoparticles by electroless plating. *Surf. Coat. Tech.* **205**, 2985 (2011).
- A. Fojtik, M. Giersig, A. Henglein. Formation of nanometer-size silicon particles in a laser induced plasma in SiH₄. *Phys. Chem.* **97**, 1493 (1993).
- H. Chen, Y. Xiao, L. Wang, Y. Yang. Silicon nanowires coated with copper layer as anode materials for lithium-ion batteries. *J. Pow. Sourc.* **196**, 6657 (2011).
- L. Hu, G. Chen. Analysis of optical absorption in silicon nanowire arrays for photovoltaic applications. *Nano Lett.* **7**, 3249 (2007).
- S. Mohapatra, Y.K. Mishra, D.K. Avasthi, D. Kabiraj, J. Ghatak, S. Varma. Synthesis of gold-silicon core-shell nanoparticles with tunable localized surface plasmon resonance. *Appl. Phys. Lett.* **92**, 103105 (2008).
- N. Dai. *Introduction to Nano Solar Cells* (Jenny Stanford Publishing, 2024).
- A. V. Krasavin, A. V. Zayats. Silicon-based plasmonic waveguides. *Opt. Exp.* **18**, 11791 (2010).
- N. O'Farrell, A. Houlton, B.R. Horrocks. Silicon nanoparticles: applications in cell biology and medicine. *Int. J. Nanomed.* **1**, 451 (2006).

28. Y. Ale, N. Nainwal. Progress and challenges in the diagnosis and treatment of brain cancer using nanotechnology *Molec. Pharmac.* **20**, 4893 (2023).
29. R. Bardhan, N.K. Grady, T. Ali, N.J. Halas. Metallic nanoshells with semiconductor cores: optical characteristics modified by core medium properties. *ACS Nano* **4**, 6169 (2010).
30. J.C. Idrobo, A. Halabica, R.H. Magruder, III, R.F. Haglund, Jr., S.J. Pennycook, S.T. Pantelides. Universal optical response of Si-Si bonds and its evolution from nanoparticles to bulk crystals. *Phys. Rev. B* **79**, 125322 (2009).
31. A.E. Miroshnichenko. Off-resonance field enhancement by spherical nanoshells. *Phys. Rev. A* **81**, 053818 (2010).
32. A.B. Evlyukhin, C. Reinhardt, A. Seidel, B.S. Luk'yanchuk, B.N. Chichkov. Optical response features of Si-nanoparticle arrays. *Phys. Rev. B* **82**, 045404 (2010).
33. C. Sönnichsen, T. Franzl, T. Wilk, G. von Plessen, J. Feldmann, O. Wilson, P. Mulvaney. Drastic reduction of plasmon damping in gold nanorods. *Phys. Rev. Lett.* **88**, 077402 (2002).
34. P. Hanarp, M. Käll, D.S. Sutherland. Optical properties of short range ordered arrays of nanometer gold disks prepared by colloidal lithography. *J. Phys. Chem. B* **107**, 5768 (2003).
35. C. Langhammer, B. Kasemo, I. Zorić. Absorption and scattering of light by Pt, Pd, Ag, and Au nanodisks: Absolute cross sections and branching ratios. *J. Chem. Phys.* **126**, 194702 (2007).
36. A.V. Korotun, N.I. Pavlyshche. Cross-sections for absorption and scattering of electromagnetic radiation by ensembles of metal nanoparticles of different shapes. *Phys. Met. Metallogr.* **122**, 941 (2021).
37. A.V. Korotun, N.I. Pavlyshche. Anisotropy of the optical properties of metal nanodisks. *Opt. Spectrosc.* **130**, 269 (2022).
38. D. Constantin. Why the aspect ratio? Shape equivalence for the extinction spectra of gold nanoparticles. *Eur. Phys. J. E* **38**, 116 (2015).
39. A.V. Korotun, Ya.V. Karandas, V.I. Reva. Analytical theory of plasmon effects in rod-shaped metal nanoparticles. Model of effective spheroid *Ukr. Fiz. Zh.* **67**, 848 (2022) (in Ukrainian).
40. A.V. Korotun, N.I. Pavlyshche. Optical absorption of a composite with randomly distributed metallic inclusions of various shapes. *Funct. Mater.* **29**, 567 (2022).
41. S. Sun, I.L. Rasskazov, P.S. Carney, P.S. Zhang, A. Moroz. The critical role of shell in enhanced fluorescence of metal-dielectric core-shell nanoparticles *J. Phys. Chem. C* **124**, 13365 (2020).
42. L.B. Lerman. Onset of additional plasmon resonances in small sheathed particles. *Poverkhnya* **14**, 91 (2008).

Received 11.02.24.

Translated from Ukrainian by O.I. Voitenko

Н.І. Павлуше, А.В. Коротун,
В.П. Курбацький, В.І. Рева

ПЛАЗМОННІ ЯВИЩА
В МЕТАЛ-ДІЕЛЕКТРИЧНИХ НАНОДИСКАХ.
ПІДХІД ЕКВІВАЛЕНТНОГО СФЕРОЇДА

В рамках підходу еквівалентного сфероїда отримано вирази для діагональних компонент тензора поляризованості та ефективності екстинкції, а також розмірних залежностей частот поздовжнього і поперечного поверхневого плазмонного резонансу для метал-діелектричних нанодисків. Наведено результати розрахунків вказаних характеристик для дисків різного розміру. Проаналізовано вплив матеріалів осердя й оболонки та розмірів диска на положення та величину максимумів ефективності екстинкції. Визначено причину виявлення тільки одного максимуму в спектрах екстинкції метал-діелектричних нанодисків.

Ключові слова: метал-діелектричний нанодиск, тензор поляризованості, ефективність екстинкції, швидкість релаксації, поверхневий плазмонний резонанс.